Superabundant microRNAs are transcribed from human rDNA spacer promoters insulated by CTCF

Steven Henikoff[1,2]* & Jorja G. Henikoff[1]

[1]Basic Science Division, Fred Hutchinson Cancer Center, Seattle, WA, USA
[2]Howard Hughes Medical Institute, Chevy Chase, MD, USA

*Corresponding author
Email: steveh@fredhutch.org

Abstract: MicroRNAs are ~22-nucleotide RNAs processed from primary transcripts and exported from the nucleus to repress gene expression by base-pairing to target mRNAs. Surprisingly, we find that the highest levels of RNA Polymerase II at human microRNA genes are within the ribosomal gene repeat arrays (rDNA) transcribed by RNA Polymerase I. Alignment of public nascent transcript data to the hs1 human genome assembly reveals a conserved 50-nucleotide foldback transcript for two microRNAs that exits from the nucleus with exceptional rapidity. We show that the miR-1275/miR-6724 transcription unit is closely flanked by CCCTC-binding factor (CTCF) within a <400-bp span of the rDNA spacer promoter. MiR-1275/miR-6724 and microRNAs expressed from the 5' External Transcribed Spacer (5'ETS) are exported independent of known RNA processing activities and are detected in exosomes and as circulating cancer biomarkers. We propose that rDNA promoter and 5'ETS microRNA genes have evolved for general regulatory functions in recipient cells.

Introduction

MicroRNAs are small non-coding RNAs that silence gene expression by base-pairing with mRNAs to prevent their translation or reduce their stability (*1*). Most microRNAs are processed from primary RNA Polymerase II (RNAPII) transcripts as hairpin structures by the Drosha Microprocessor complex and exported from the nucleus, where the hairpin is cleaved by Dicer, and the processed microRNA is bound by an Argonaute protein. Some microRNAs are released from the cell within extracellular vesicles and taken up by recipient cells where they have been observed to alter gene expression (*2*).

Many different microRNAs have been implicated in cancer, where they may regulate tumor suppressor or oncogene expression (*3-6*). The high abundance of circulating microRNAs indicates that these are likely expressed at especially high levels and rapidly exported. However, the small size and rapid processing of microRNAs make them difficult to detect in clinical samples by standard RNA-sequencing (RNA-seq). Instead, microarray-based targeted assays are frequently used for cancer diagnostics (*7, 8*) as a substitute for deep sequencing of small RNAs (*9-11*). MicroRNA abundances can also be estimated using Cleavage Under Targeted Accessible Chromatin (CUTAC) with antibodies to RNAPII in formalin-fixed paraffin-embedded (FFPE) sections (*12*). Using FFPE-CUTAC, we have shown that the conserved neural-specific miR-124a microRNA is abundantly expressed in normal mouse brain but strongly down-regulated in gliomas, a difference that was undetectable by RNA-seq. This finding encourages the expanded use of FFPE-CUTAC for microRNA detection in clinical applications, including cancer diagnosis, where a single assay will sensitively detect transcription of all RNAs, including mRNAs, microRNAs and other RNAs not easily detected in FFPEs.

Examination of our published human FFPE-CUTAC data revealed that a few microRNA loci consistently showed the highest RNAPII-Serine-5p (RNAPII-S5p) signals in all tissues and tumors tested when aligned to the hg19 or hg38 human genomic assemblies, where Serine-5 phosphorylation of the Rbp1 C-terminal domain marks RNAPII that is paused before release for productive elongation (*13*). By aligning these microRNA genes to the full chm13 genome assembly we show that these and several other microRNAs are transcribed from the >200 ribosomal DNA repeats that reside on the short p arm of acrocentric chromosomes. Analysis of published run-on, nascent and small RNA sequencing data revealed that these microRNAs are exported within minutes after release from the DNA template and are not processed by Drosha or Dicer. Remarkably, expression of a conserved 50-nucleotide foldback transcript for two microRNAs is insulated by CCCTC-binding factor (CTCF) within the ribosomal DNA (rDNA) spacer promoter and exported with exceptional rapidity, independent of known RNA processing activities. Both miR-1275 and miR-6724 are abundant in exosomes and are the most differentially upregulated microRNAs in multiple human cancers. Our results suggest that rDNA promoter and downstream microRNAs have evolved for gene regulatory functions within recipient cells.

Results

Paused RNA Polymerase II is superabundant at microRNA genes within human ribosomal DNA repeats

We previously applied RNAPII-S5p CUTAC to FFPEs from cancer patient samples representing seven diverse cancer types, and ranked candidate *cis*-regulatory elements (cCREs) by plotting the difference between tumor and normal samples as a function of the average on a $\log_{10}$ scale (modified Bland-Altman plots) (*13*). Unexpectedly, three cCREs representing miR-663A were consistently the highest in overall abundance for all seven patients, showing little if any difference between tumor and normal samples (**Fig. 1A**). As miR-663A expresses a microRNA, we rank-ordered RNAPII CUTAC signal over the 2,011 non-overlapping human microRNAs in RefSeq, which revealed that miR-663A ranks third behind miR-3648 and miR-10396 for all seven tumor and normal patient samples (**Fig. 1B**).

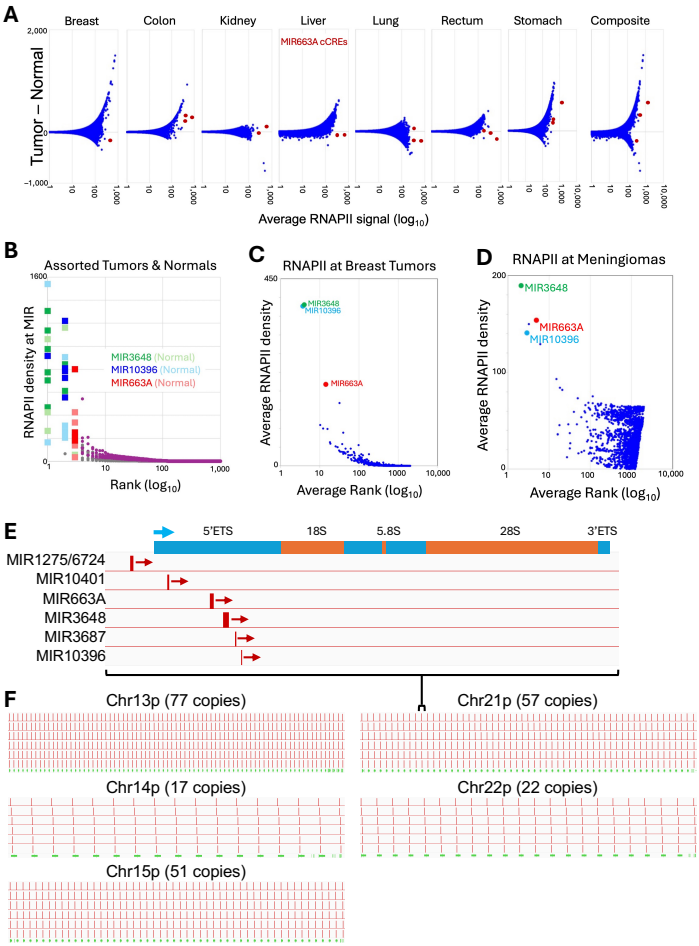

Fig. 1: RNAPII is superabundant at three microRNA genes in cancer and normal cells. (**A**) Modified Bland-Altman plots (*22*) of RNAPII FFPE-CUTAC data for 984,834 human cCREs from the ENCODE project (*23*) from seven matched tumor and normal patient samples. MiR-663A is highlighted with up to three cCREs that show the highest average abundance but with no consistent differences between tumor and normal. (**B**) RNAPII FFPE-CUTAC data were aligned to RefSeq-annotated microRNAs and rank-ordered, with miR-3648, miR-10396 and miR-663A ranked the highest with no consistent differences between tumor and normal. Ranks were averaged for patient samples from 15 breast tumors (**C**) and 30 meningiomas (**D**) and the averages were plotted as a function of RNAPII density, showing that the same three microRNA genes were consistently among the top three. Neither miR-3648 nor miR-10396 is represented by a cCRE, which accounts for their absence from the Bland-Altman plots in (A). (**E**) Alignment of miRBase-annotated microRNAs within the promoter and 5'ETS of the ribosomal genes for a representative repeat unit within Chromosome 21. (**F**) MegaBLAST (*24*) was used to align microRNA sequences to hs1, which mapped them to each of the 224 repeat units in the hs1 genomic assembly.

We also ranked RNAPII signal at microRNA sequences for the other FFPE-CUTAC samples from our previous study (*13*), plotting the average ranks for 15 breast and 30 meningioma patient samples, and again observed that miR-3648, miR-10396 and miR-663A were consistently the top three microRNA loci based on RNAPII-S5p abundance (**Fig. 1C-D**).

RefSeq annotations for the hg38 genome assembly (*14*) place miR-3648 and miR-10396 on Chromosome 21p, the short p arm of one of the five human acrocentric chromosomes, each of which harbors a tandem repeat array of ribosomal RNA (rRNA) genes. In late 2021, the Telomere-to-Telomere (T2T) project released full genomic assemblies that resolved the tandemly repetitive satellite, telomeric and ribosomal gene arrays using long-read sequencing and improved genome assembly algorithms applied to the homozygous chm13 cell line (*15, 16*). When we aligned the three microRNAs with superabundant RNAPII-S5p to the chm13 (hs1) genome assembly we found that all of them are located within the 5' External Transcribed Spacer (5'ETS) of the ribosomal gene arrays (**Fig. 1E**). This implies that RNAPII is not superabundant over these loci but rather is present at merely high abundance on a per locus basis, with the signal amplified by the 224 rDNA copies annotated in the chm13 cell line (**Fig. 1F**). miR-663A and miR-3648 were previously identified as residing within the 5'ETS by Yoshikawa and Fujii, who had searched miRBase (*17*) entries against a single ribosomal DNA (rDNA) repeat unit (*18*). We confirmed their findings, adding miR-10396 and miR-10401 which were more recently annotated in miRBase (*17*). In total, at least five annotated microRNA genes reside in the 5'ETS, with miR-1275 and miR-6724 just upstream.

A ribosomal DNA spacer promoter transcript rapidly exits from the nucleus

To obtain a profile of transcription that is not biased by RNA processing and does not depend on the particular RNA polymerase responsible, we aligned nascent transcription data to the hs1 genome assembly (*16*). We first analyzed data generated in various studies using PRO-seq, an *in vitro* "run-on" method that maps the RNA base in the active site of transcriptionally engaged RNA polymerases (*19*). By aligning PRO-seq data from the chm13 cell line to the hs1 assembly we observed a single sharply defined peak over each of the five acrocentric short arms, transcriptionally oriented 5'-to-3' from telomere to centromere (**Fig. 2A**). Expansions of the scale for Chromosome 21 confirmed that the peak corresponded to the rDNA repeat array within Chr21p12 and that each rDNA repeat unit showed strong PRO-seq signals over the transcribed region (**Fig. 2C-E**). As ~80% of transcription in the human genome is of the ribosomal genes (*20*), such extreme abundance of run-on transcription over the ribosomal RNA transcription was not unexpected. To confirm this *in vivo*, we turned to TT-seq, in which nascent RNA is pulse-labeled for ~5 minutes with 4-thiouridine (4sU) followed by fragmentation, purification and sequencing of 4sU RNA (*21*). Using data from the DLD-1 colorectal adenocarcinoma cell line we observed the same five sharp peaks over the short p arms of the acrocentric chromosomes (*25*) (**Fig. 2B**). These cells had been treated with 5,6-dichlorobenzimidazole (DRB), which inhibits the Cdk9 kinase of pTEFb, important for productive elongation, consistent with enrichment of paused RNAPII at rDNA promoter and ETS microRNAs (**Fig. 1A-D**).

A conspicuous feature of the chm13 PRO-seq profile over the rRNA repeat unit is a sharp upstream peak that spans miR-1275 and miR-6724 (**Fig. 2E**). A similar pattern is

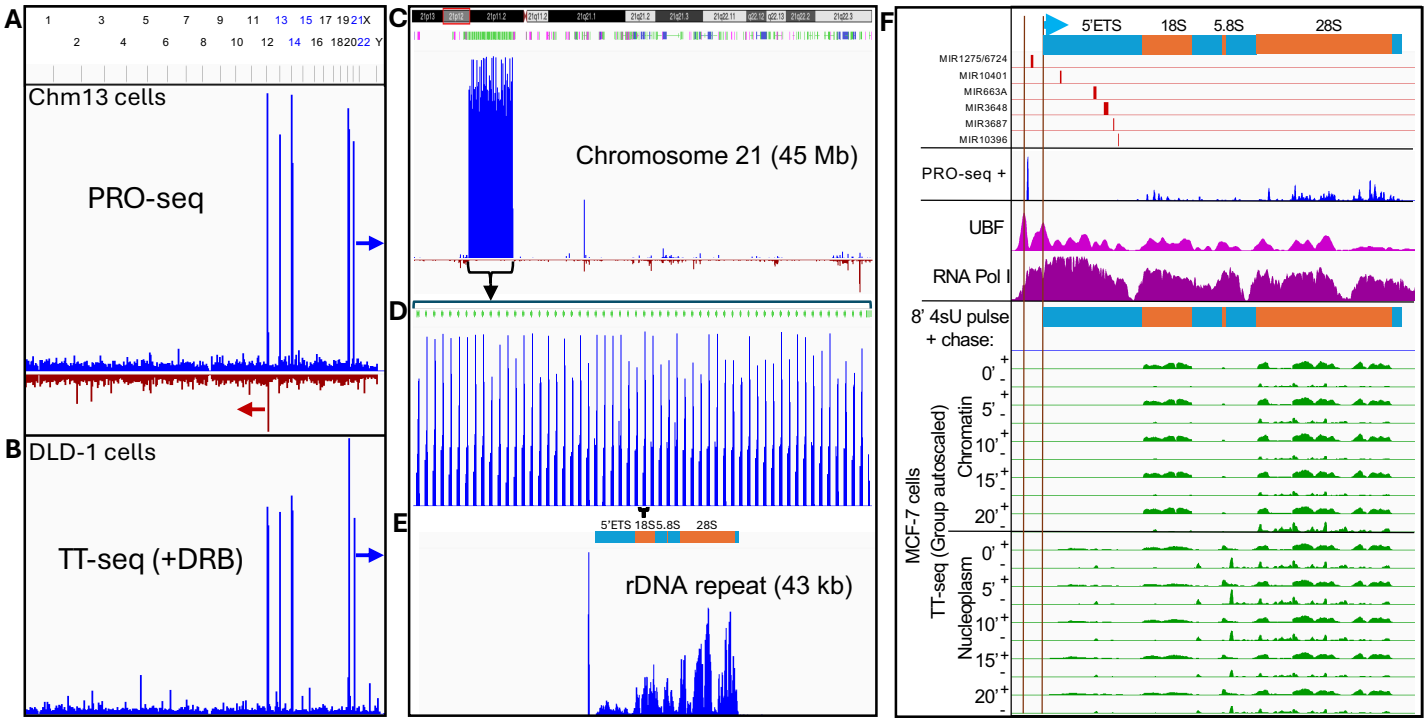

Fig. 2: A ribosomal DNA spacer promoter transcript rapidly exits from the nucleus. (**A**) PRO-seq profiles from the chm13 cell line shows strong peaks over the five human acrocentric chromosomes when aligned to hs1. The arrows indicate direction of transcription. (**B**) TT-seq data from DLD-1 cells confirms the PRO-seq forward strand profile *in vivo*. (**C**) The mini-chromosome from the hs1 assembly locates the strong PRO-seq peak over the hs1-annotated rDNA genes (green) within Chr21p12 (chr21:3,544,445-3,585,713). (**D**) Expansion of the Chr21 rDNA region. (**E**) Expansion of a single rDNA repeat unit centered over the transcribed region. (**F**) Top: Location of microRNA genes relative to the 47S rRNA precursor map within a representative rDNA repeat unit (chr21:3,544,445-3,585,713). Chm13 PRO-seq data (*16*) (blue), UBF and RNAPI ChIP-seq data (purple) and chrTT-seq pulse-chase data (*28*) below (green). Vertical lines indicate UBP promoter peaks that mark the spacer and 47S promoters (*30*).

observed over the rDNA repeat unit for PRO-seq data from Kasumi-1, a myeloblast cell line (*26*) (**Fig. S1F–1-2**). The run-on and pulse-labeled transcripts over the ribosomal genes correspond to high levels of the Upstream Binding Factor (UBF) and RNAPI (*27*) (**Fig. S1F–3-4**) and low levels of RNAPII (**Fig. S1F–5-8**), as expected for transcription of the active rDNA genes by RNAPI and repressive RNAPII transcription of the inactive rDNA genes (*28*). The miR-1275/6724 PRO-seq peak lies within the UBF-defined rDNA promoter. Total RNA-seq signal was high over 18S, 5.8S and 28S regions corresponding to stable transcripts (*10*) (**Fig. S1F–9-10**), however DRB-resistant chromatin-enriched RNA (cheRNA) was abundant primarily over the 5'ETS (*29*) (**Fig. S1F–11-12**), consistent with rapid degradation of rRNA transcribed spacers.

To distinguish RNA polymerase release and export from programmed degradation, we examined TT-seq pulse-chase data from the MCF-7 breast cancer cell line, in which chromatin-bound and nucleoplasmic RNA fractions were sequenced separately (*28*). After an 8' pulse of 4sU, the 18S, 5.8S and 28S regions show strong TT-seq signal in both fractions, and the 5'ETS region shows only nucleoplasmic RNA signal, however there is no TT-seq signal within the promoter and 5'ETS regions in the chromatin fraction (**Fig. 2F-G**). This suggests that the nascent run-on transcripts corresponding to rDNA promoter microRNAs were already exported from the nucleus before the end of the 8' pulse. Transcripts on the opposite strand are seen throughout the 47S precursor region and may result from low levels of RNAPII transcription that have been observed to occur over silenced rDNA repeats (*27*). We infer that the abundant promoter microRNA transcripts observed in PRO-seq data are exported out of the nucleus within minutes, and the absence of TT-seq chromatin signal in the 5'ETS region suggests that these microRNAs are rapidly exported as well.

CTCF insulates the spacer promoter|miR-1275/6724 transcription unit

Zentner and co-workers mapped the CTCF transcription factor (TF) to the rDNA "spacer" promoter, very close to the location of miR-1275/6724 (*31*). To determine the precise location of this CTCF peak relative to miR-1275/6724 promoter, we analyzed DFF-ChIP data, in which native chromatin is fragmented using a non-specific double-strand endonuclease followed by immunoprecipitation (*32*). We separated fragments by size to distinguish CTCF that is directly bound to DNA (≤120 bp) from nucleosome-bound CTCF (>120 bp), (*33*). We also plotted native DFF-ChIP data for TATA-binding protein (TBP) (*34*), where previous work has shown TBP peaks over both the 47S rRNA promoter and the upstream "spacer" promoter corresponding to UBF peaks (*35*). We observed that directly bound CTCF maps both immediately upstream of TBP, and immediately downstream of the miR-1275/6724 PRO-seq

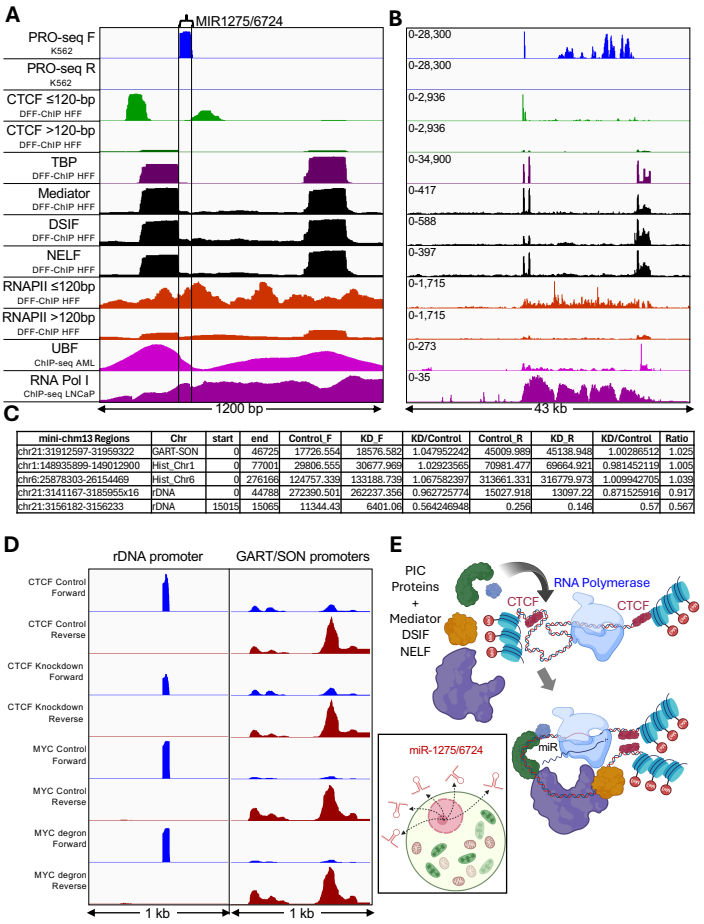

mini-chm13 Regions	Chr	start	end	Control_F	KD_F	KD/Control	Control_R	KD_R	KD/Control	Ratio
chr21:31912597-31959322	GART-SON	0	46725	17726.554	18576.582	1.047952242	45009.989	45138.948	1.00286512	1.025
chr1:148935899-149012900	Hist_Chr1	0	77001	29806.555	30677.969	1.02923565	70981.477	69664.921	0.981452119	1.005
chr6:25878303-26154469	Hist_Chr6	0	276166	124757.339	133188.739	1.067582397	313661.331	316779.973	1.009942705	1.039
chr21:3141167-3185955x16	rDNA	0	44788	272390.501	262237.356	0.962725774	15027.918	13097.22	0.871525916	0.917
chr21:3156182-3156233	rDNA	15015	15065	11344.43	6401.06	0.564246948	0.256	0.146	0.57	0.567

Fig. 3: DFF-ChIP reveals precisely coordinated factors in the spacer promoter. (**A**) DFF-ChIP fragments from human foreskin fibroblast cells were aligned over the region spanning the rDNA spacer and 47S promoters, revealing the precise positioning of CTCF (green), TBP (purple), Mediator, DSIF and NELF (black) and RNAPII (orange) relative to miR-1275/6724, UBF and RNA Pol I (vertical lines). (**B**) Same as (A) showing the full rDNA repeat unit and scale. (**C**) CTCF Knockdown reduces total PRO-seq signal over miR-1275/6724 but has no effect on housekeeping control genes. Total PRO-seq signal for each strand was summed over entire mini-chromosomes and the fold-change was calculated for each strand and averaged for an overall ratio (last column). Controls were the GART-SON region (Ratio = 1.025), the histone gene cluster on Chr1 (Hist_Chr1 (Ratio = 1.005) and the histone gene cluster on Chr6 (Hist_Chr6 (Ratio = 1.039). A minor reduction with knockdown is seen for the entire rDNA repeat (Ratio = 0.917), and a substantial reduction for miR-1275/6724 (Ratio = 0.567). (**D**) Group-autoscaled PRO-seq profiles for 1-kb regions including the miR-1275/6724 promoter (left) and the bidirectional GART-SON promoter (right) ± depletion of CTCF or MYC. (**E**) Model in which CTCF (with cohesion, not shown) insulates the <400-bp spacer promoter from H3K27me3-marked nucleosomes on silenced copies and/or UBF on active rDNA copies, allowing for unimpeded PIC assembly and RNA polymerase engagement. The image was created with BioRender.com.

signal (**Fig. 3A-B**). We also plotted native DFF-ChIP fragments for RNAPII-specific accessory factors, Mediator, DSIF and NELF, and observed precise co-localization with TBP over both spacer and 47S promoters, confirming that both promoters are active, although whether on the same or different rDNA copies could not be determined. Remarkably, the precisely defined squared-off DFF-seq peaks suggest that the promoter elements (TBP-Mediator-DSIF-NELF) closely abut the RNA polymerase defined by PRO-seq, and CTCF is juxtaposed just upstream of the promoter and downstream of the RNA polymerase, all within <400 bp.

To further characterize the rDNA promoter region, we aligned ATAC-seq data from Kasumi-1 cells and observed a peak centered over TBP-defined spacer promoter, presumably from UBF-bound active copies (**Fig. S2**). We also observed a TBP-centered peak of H3K27me3 with low-level H3K27ac in prostate cancer metastases, presumably from nucleosome-bound inactive copies. Additionally, we aligned CUT&RUN data for the MYC oncogene, which is known to upregulate rDNA genes in mammals (*36, 37*) and Drosophila (*38*), and observed that in K562 cells, MYC and its partner MAX peak over the spacer promoter, as did the JUN TF in Hct116 cells (**Fig. S2**).

To test whether CTCF is functionally important for miR-1275/6724 transcription, we examined CTCF knockdown data (*39*). This showed no effect on PRO-seq signal over housekeeping gene loci (KD/Control = 1.01-1.03), a minor reduction over the rDNA repeat unit (0.92) and a substantial reduction over the 50-bp miR-1275/6724 locus (0.57), whereas degron-targeting of MYC showed little reduction of the miR-1275/6724 PRO-seq signal (**Fig. 3C-D**). Based on these observations from multiple cell lines, we infer that CTCF binding both immediately upstream of the spacer promoter and downstream of miR-1275/6724 insulates this intensely transcribed <400-bp region from nucleosome and/or UBF encroachment on either side (**Fig. 3E**). Consistent with this interpretation, the Cohesin complex was found to co-localize with the upstream peak (*30*), centered over the Zentner *et al.* CTCF motif (*31*) in the "forward" orientation for boundary pairing (*40*). The downstream peak spans an 83% G/C region with multiple regions potentially permissive for CTCF binding (*41*).

MiR-1275/6724 is regulated independently of the rDNA

If CTCF functions to insulate miR-1275/6724, then it might also function to enforce independent regulation of the spacer promoter from the 47S rRNA promoter. To test this possibility, we first asked whether miR-1275/6724 uses a different RNA polymerase from RNAPI, which transcribes the 47S rRNA genes. Alignment of RNAPII high-resolution native DFF-seq fragments over the promoter region showed similar RNAPII occupancy around both the spacer and 47S promoters extending through the entire transcribed rDNA, similar to what is observed for RNAPI ChIP-seq (**Fig. 3A**). To test for possible RNAPII transcription of miR1275/6724, we asked whether Triptolide, which inhibits the catalytic activity of the RNAPII-specific translocase complex, TFIIH, also reduces the miR-1275/6724 PRO-seq signal. Using data from a recent study in K562 cells (*42*), we observed 1.4-2.1 fold increases depending on Triptolide concentration and treatment time for miR-1275/6724, with only slight changes up or down for 47S transcription (**Fig. 4A**), whereas control GART-SON housekeeping gene promoters showed

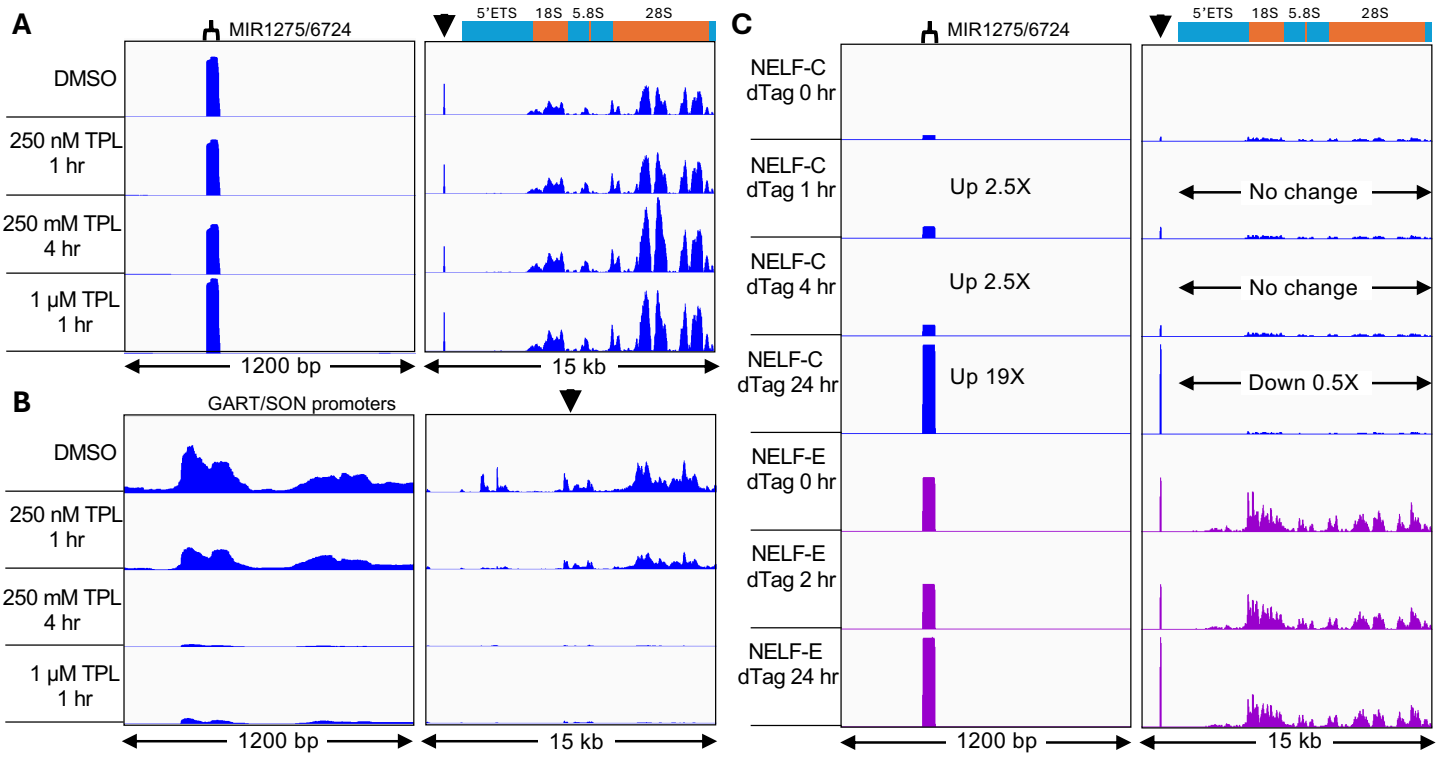

Fig. 4: MiR-1275/6724 is regulated independently of the rDNA. PRO-seq data for RNAPII inhibition and NELF degradation. Group-autoscaled within series. (**A**) K562 cells (*42*) were treated with Triptolide (TPL) at the indicate concentration and time, showing the rDNA promoter (left) and transcribed regions (right). (**B**) Same as (A) except for the control GART/SON promoter region (left) and zoomed out to 15 kb (right). (**C**) HFF cells had been transformed with NELF dTag constructs which were activated for degradation for the indicated times (*45*). NELF-C (blue) and NELF-E (magenta).

drastic ~30-fold reductions at the higher levels of inhibition (**Fig. 4B**). Increased PRO-seq signal with Triptolide treatment was also seen in that study for certain long non-coding RNAs, consistent with classical *in vitro* reconstitution and recent cryoEM studies showing that TFIIH is not needed for promoter opening under torsional conditions favorable for spontaneous denaturation (*43, 44*). This may explain the evident juxtaposition of TBP-Mediator-DSIF-NELF with RNA polymerase at miR-1275/6724, where there is no free DNA available for action of the TFIIH translocase.

Another RNAPII-specific inhibitor is Flavopiridol, which like DRB, inhibits pTEFb, reducing productive elongation. When we analyzed PRO-seq data from human foreskin fibroblast (HFF) cells treated with Flavopiridol (*34*), we observed a 3.5-fold reduction at miR1275/6724 (**Fig. S3A**) and an ~10-fold reduction of the GART-SON control promoters (**Fig. S3C**). In contrast, the signal over the transcribed rDNA increased 1.5-fold (**Fig. S3B**). The authors of this study also depleted TATA-binding protein (TBP) using a degron system over a 4-72 hour range (*34*), and we observed substantial increases in PRO-seq signal after Flavopiridol treatment for miR-1275/6724 and GART-SON but decreases for rDNA (**Fig. S3**). Taken together, these observations imply that miR-1275/6724 is regulated independently of the ribosomal genes.

We next asked whether dTag depletion of the Negative Elongation Factor NELF would differentially affect miR-1275/6724 and rDNA transcription. Indeed, based on DLD-1 cell line data, we observed a 2.5-fold increase in miR-1275/6724 PRO-seq signal after a 1 hour dTag depletion of the NELF-C subunit, and 19-fold after 24 hours, by which time the rDNA PRO-seq signal had decreased by 50% (**Fig. 4C**). dTag depletion of NELF-E also increased the PRO-seq signal ~2-fold without affecting the rDNA signal. These observations further demonstrate that miR-1275/6724 is regulated independently of the ribosomal RNA genes. The consistent opposite effects on miR-1275/6724 and 47S transcription caused by inhibition of pTEFb and depletion of NELF, both of which are RNAPII-specific initiation factors, strongly suggests that RNAPII transcribes miR-1275/6724.

The 50-nt rDNA spacer promoter microRNA precursor is conserved in primates

To determine the precise length of the miR-1275/6724 transcript, we compared the PRO-seq profile to the PRO-cap profile from the same DLD-1 cell line, where PRO-cap maps the modified 5'-end of the nascent transcript. We found that ~95% of 5'-ends align precisely at the annotated 5'-end of miR-1275 and half of them have 3' ends precisely at the 3' end of miR-6724, consistent with the PRO-seq profile (**Fig. 5A**). The lack of excess nucleotides on either end implies that a 50-nucleotide microRNA precursor for miR-1275 and miR-6724 is a primary transcript that does not require Drosha cleavage activity of the Microprocessor complex.

A previous study identified miR-3638, miR-10396 and miR-6724 genes from hg38, where they had appeared to be uniquely present on Chromosome 21 (*47*). The authors'

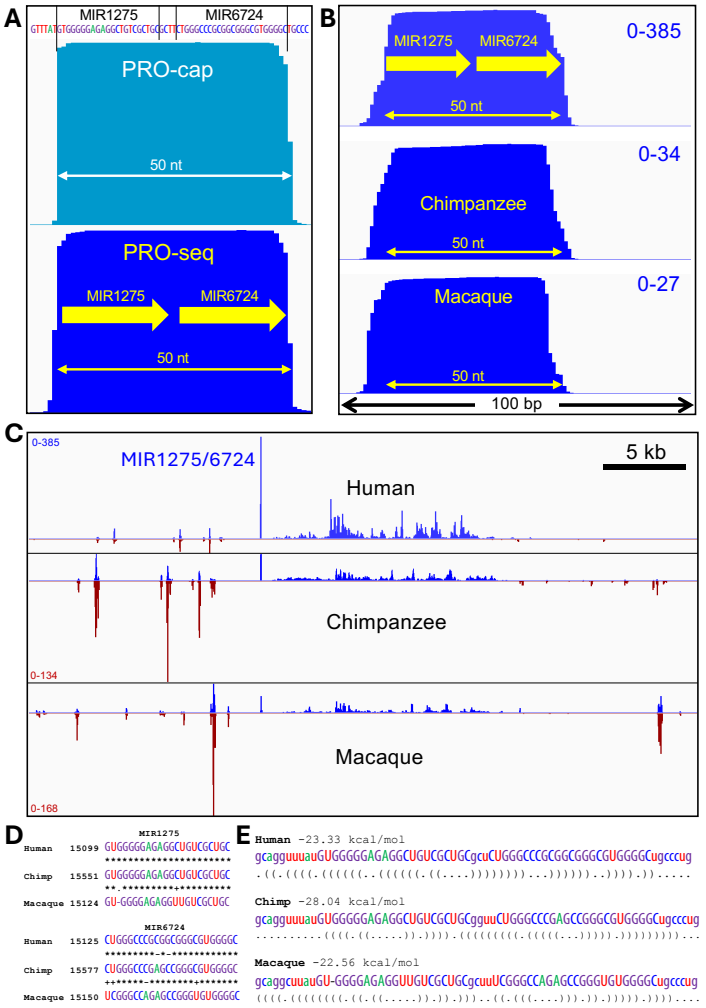

Fig. 5: A conserved 50-nt rDNA promoter microRNA precursor. (**A**) Forward-strand PRO-cap (turquoise) and PRO-seq (blue) mini-chromosome data for the rDNA promoter transcription unit (*45*). (**B**) A 100-bp region including the miR-1275/6724 peak at high resolution aligned by sequence similarity showing the + strand. (**C**) Forward-strand (blue) and reverse-strand (brown) PRO-seq data (*46*) for a representative rDNA repeat unit (chr21:3,141,168-3,185,955) aligned with the corresponding regions of the chimpanzee rDNA repeat (GenBank KX061886.1) and the rhesus macaque rDNA repeat (KX061890.1) from CD4(+) T-cells. (**D**) Species alignments of the two microRNAs where each transition is indicated with a + and transversion or gap with a -. (**E**) The 50-bp human rDNA promoter foldback structure is shown in Vienna format for each of the species.

analysis of this region in ape and ancient human genomic assemblies at the time led them to suggest that this region of Chr21p11 emerged *de novo* in the human genome. Recently, Telomere-to-Telomere assemblies have been produced for several primates (*47*), which provide the opportunity to test whether the rDNA microRNAs have been conserved over evolutionary time. We aligned existing PRO-seq data from chimpanzee and rhesus macaque (*46*) to their corresponding genome assemblies and observed that both species' peaks precisely span the 50-nt miR-1275/6724 hairpin (**Fig. 5B-C**). There are few polymorphic differences between species (**Fig. 5D**), and the foldback structures that are substrates for cleavage and release to Argonaute proteins for translational regulation are also conserved (**Fig. 5E**), with similar minimum free energies of folding for all three species (~20 kcal/mol) (*48*). The minimum free energies of foldback structures for microRNAs in the 5'ETS region are also similar between species (**Fig. S4**). We conclude that the microRNA cluster within the human ribosomal repeats has been functional at least since the last common ancestor of humans and macaques, ~25 million years ago.

Evolutionary conservation of the rDNA promoter microRNAs makes it most probable that they evolved to serve a housekeeping function requiring the high levels of transcript production that is possible with all >200 RNAPI promoters producing the same transcript. For example, microRNAs found in extracellular vesicles have been shown to mediate changes in gene expression within recipient cells and are suspected in some cases to transmit drug resistance (*49*), where high abundance would give a microRNA-producing cell a competitive advantage. It is also possible that spacer promoter transcription serves as a CTCF-regulated switching mechanism that maintains the balance between active and silent rDNA copies to respond to external signals, with the production and rapid export of miR-1275/6724 serving subsequent functions in recipient cells. These roles are not mutually exclusive.

rDNA chromatin and euchromatin levels are anti-correlated

Human rDNA copy numbers vary up to a few-fold between individuals (mean 469 ± 107) (*50, 51*), and we wondered whether rDNA copy number instability (*20, 52*) could be responsible for the discrepancies between levels of the rDNA promoter transcripts and both RNAPI- and RNAPII-dependent transcripts in response to different perturbations. To explore this possibility, we asked whether stable chromatin and transcriptional marks show concordance between the rDNA and other highly active loci in end-stage prostate cancer (*53*). In the case of H3K27me3, a mark of Polycomb silencing, we observed that their CUT&Tag signals over rDNA and euchromatin on Chr1q transcribed by RNAPII were almost perfectly *anti-correlated* ($r = -0.999$, $p < 0.00001$), whereas the histone gene clusters and the GART-SON housekeeping control regions were positively correlated with one another as expected ($r = 0.377$ to 0.732, **Fig. 6A, 6E**). Similarly, strong anti-correlations between rDNA and Chr1q euchromatin were seen for the active H3K27ac mark ($r = -0.841$, $p < 0.00001$, **Fig. 6B, 6F**) and for RNAPII-Ser5p signal from our FFPE-CUTAC data for multiple replicates from 13 breast tumors (–0.705, $p = 0.0003$, **Fig. 6C, 6G**) and 30 mostly benign meningiomas (–0.782, $p < 0.00001$, **Fig. 6D, 6H**). Such exceptionally strong anti-correlations for RNAPI-transcribed rDNAs and RNAPII-transcribed euchromatin for both active and silencing chromatin marks and paused RNAPII is most easily understood if they reflect rDNA copy number differences between patients. We suggest that the variability that we observed in perturbation experiments described above are likewise attributable in part to rDNA copy number variation.

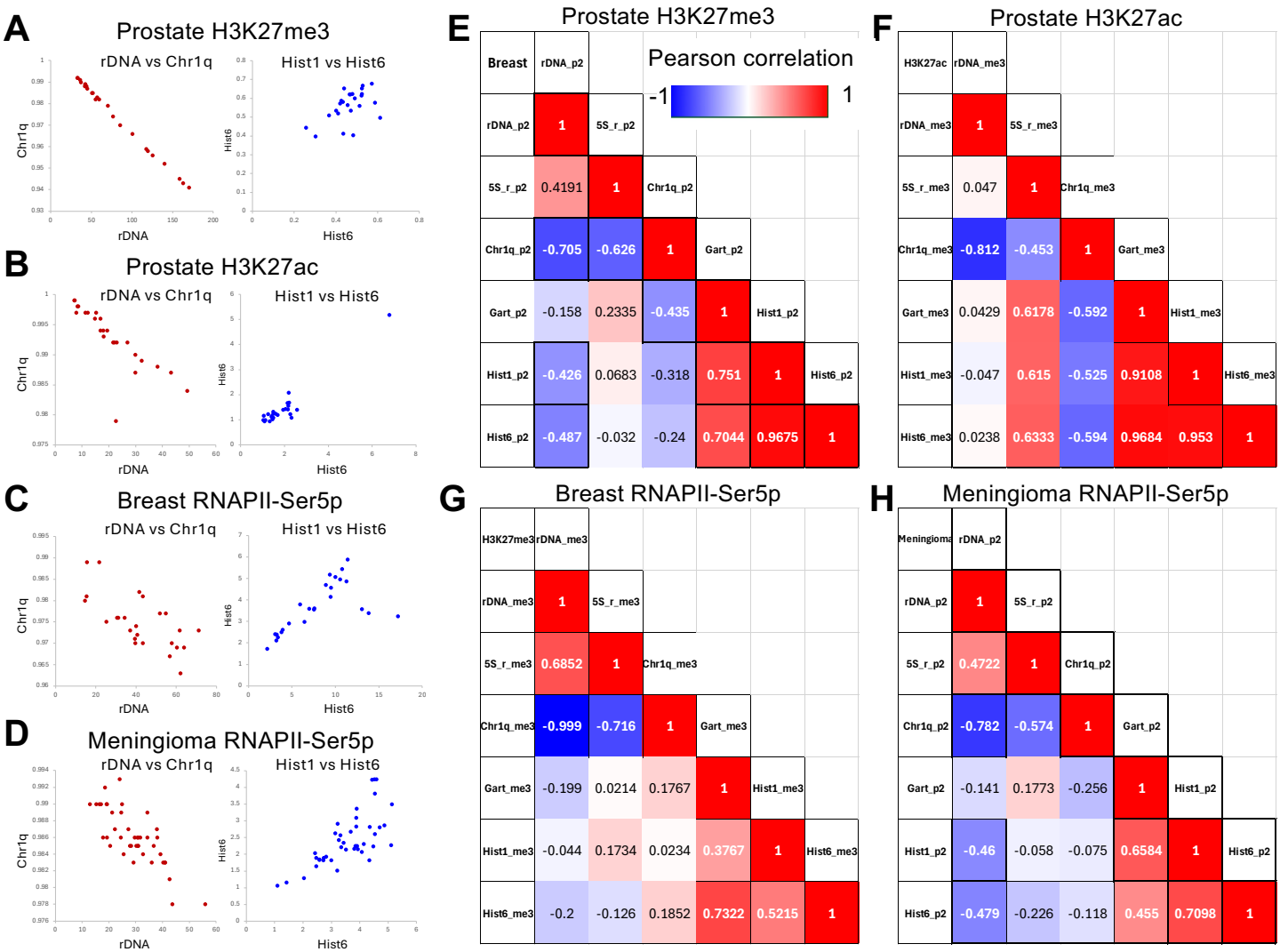

Fig. 6: Ribosomal DNA and euchromatin are anticorrelated for chromatin and RNAPII marks. The human rDNA genes are almost perfectly anti-correlated with Chr1p euchromatin, from which the Hist1 cluster and the RNA5S cluster have been removed. (**A-B, E-F**) Correlation matrices for chromatin profiles of the silencing H3K27me3 mark (r = –0.999) and the active H3K27ac mark (r = –0.812) in multiple replicates from eight end-stage prostate cancer metastases. CUT&Tag patient data are from GSM8791938-GSM8791987 (*53*) (**Fig. S5**). Significant anti-correlations are also seen for multiple replicates of RNAPII-Ser5p in (**C, G**) 13 primary breast tumors (r = –0.705) and (**D, H**) 30 meningiomas (r - –0.782) and between RNA5S and euchromatin (r = –0.453 to –0.782, p = 0.02 to 0.00006). In contrast, the Chr1 and Chr6 histone gene clusters are positively correlated with one another and with the control GART-SON locus in most other comparisons. FFPE-CUTAC data from Ref. (*13*).

We also observed significant anti-correlations in patient data between the 5S ribosomal DNA genes, which are transcribed by RNAPIII, and Chr1q (r = –0.453 to –0.782, p = 0.02 to < 0.00001, **Fig. 6E-H**), even though this cluster of 101 active RNAPIII transcribed genes reside on Chr1q. The significant positive correlation between rDNA and the 5S DNA for H3K27me3 (r = –0.69, p = 0.0002) and their anti-correlations with Chr1q euchromatin suggests that the two polymerases transcribing ribosomal genes compete against RNAPII for limiting nucleoside triphosphates.

The MiR-1275/6724 transcript uses a non-canonical processing pathway

Most RNAPII microRNA hairpin precursors are excised during transcription and are exported to the cytoplasm where the functional microRNA is released (*54*). However, a recent study reported that microRNAs processed by RNA Polymerase III (RNAPIII) use a non-canonical pathway and are insensitive to inhibitors of the Microprocessor and Dicer (*55*). To determine whether rDNA promoter microRNAs are processed by the Microprocessor and Dicer, we aligned the small-RNA sequencing data from that study to the hs1 assembly and compared the profiles of rDNA microRNAs to that of miR-4521, which uses a non-canonical pathway. Inhibition of RNAPIII, which caused strong down-regulation of miR-4521, resulted in upregulation of the rDNA promoter microRNAs, miR-1275 and miR-6724 (**Fig. 6**). Upregulation with RNAPIII inhibition was also observed for the 5'ETS microRNAs, miR-10401 and miR-4466, which are predicted to form a tight hairpin structure (**Fig. S5**). This opposite response to RNAPIII inhibition for rDNA microRNAs appears to be general, as two pairs of putative miRs in the 5'ETS not annotated in miRBase also show upregulation with RNAPIII inhibition (**Fig. 7**). Upregulation of miR-1275/6724 with reduction of RNAPIII is consistent with competition between

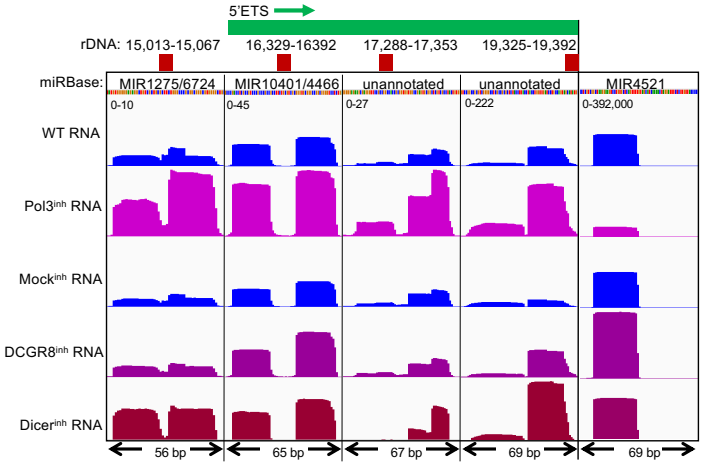

Fig. 7: Processed microRNAs from the rDNA promoter and 5'ETS use a non-canonical processing pathway. Total small-RNA sequencing data were aligned to a representative human rDNA repeat unit (chr21:3,141,168-3,185,955) and displayed in IGV format (*56*), group-autoscaled for the five tracks, where the positions within the promoter-5'ETS region are shown and spans are indicated above. The scales range from 0-10 for miR-1275/6724 to 0-392,000 for miR-4521, consistent with rapid export of miR-1275/6724 from cells. Inhibition of the DCGR8 Microprocessor subunit and the Dicer enzyme indicates that nearly all of these microRNAs do not use the canonical processing pathways.

RNA polymerases for limited nucleoside triphosphates as suggested above.

Notably, the abundance of miR1275/6724 is ~1/40,000th that of miR-4521 and 5' ETS microRNAs are also orders of magnitude less abundant (**Fig. 7**). This is consistent with the amounts of rDNA-derived non-coding RNAs measured at <1/10,000th the concentration of rRNA (*27*). We suggest that rapid export of primary transcripts from the cell and uptake by recipient cells can account for the low levels of processed rDNA spacer promoter and 5'ETS microRNAs relative to the level of miR-4521.

Inhibition of DCGR8, a subunit of the Microprocessor complex (*54*), resulted in strong upregulation of miR-4521, and moderate upregulation of miR-1275, miR-6724, miR-10401 and miR-4466, although the effect on the unannotated transcripts varied from little or no effect to strong upregulation (**Fig. 7**). Similarly, the effect of inhibiting Dicer resulted in upregulation of miR-4521 and variable effects on the RNAPI-generated transcripts, with only one of the four unannotated microRNAs showing downregulation. We conclude that the annotated microRNAs transcribed from the rDNA promoter and 5'ETS are both Microprocessor- and Dicer-independent, using a non-canonical pathway for export and excision from the primary transcripts.

Discussion

We have uncovered a unique mode of transcriptional regulation, in which the ribosomal gene spacer promoter is the source of a conserved 50-nt foldback nascent transcript detected at exceptionally high levels in human cells. Although our evidence is based on data that have been publicly available for years, we are not aware of any previous report of rDNA promoter transcripts in any organism. This oversight may be attributable in part to the fact that rRNA is by far the most serious contaminant of mRNAs in RNA sequencing studies, and standard protocols and analytical methods are designed to exclude it. Furthermore, the ribosomal genes have been deleted or masked in widely used eukaryotic genome assemblies and only with the hs1 genome assembly has it been possible to capture the full arrays on the short arms of all five human acrocentric chromosomes. Although the hs1 assembly has been available for ~4 years, there are relatively few non-repetitive genes present in regions that are absent from previous genome assemblies, and so there has been little incentive to switch to it. Indeed, we only noticed the superabundance of rDNA microRNAs as a puzzling anomaly in Bland-Altman plots, which required the full hs1 assembly to resolve. Overall, only 664 (1%) of Gene Expression Omnibus entries are aligned to hs1, compared to 26,133 for hg19 and 41,558 for hg38. Also, the small size and biased base composition of microRNAs result in their being attributed to single copy sequences that may occur by chance; for example, miR-1275 is annotated as a gene in Chromosome 6 euchromatin (*17*) based on detection of a G-rich 17-bp RNA by small-RNA sequencing (*57*).

Multiple lines of evidence suggest that this novel rDNA spacer promoter transcript is rapidly exported from the nucleus: 1) Despite showing the highest density of any nascent transcript in the rDNA by run-on transcription, transcription of the region is undetectable in both the chromatin-bound and the nucleoplasmic fractions after an 8 minute pulse of 4sU; 2) The two stable cleavage products of the 50-bp rDNA promoter transcript, miR-1275 and miR-6724, are detectable in cells at a level that is more than four orders of magnitude lower than that of miR-4521; 3) Both miR-1275 and miR-6724 have been recovered from exosomes and miR-1275 is abundant in human tissues, serum and urine (*7-9*).

Several other microRNA transcripts are expressed from within the 5'ETS region, including miR-10401, miR-4466, miR-663a, miR-3648, miR-3687 and miR-10396, as well as four putative microRNAs not annotated in miRBase. As these are all transcribed from the same strand as the 5'ETS, they may have been excised from primary rRNA transcripts. Like rDNA promoter microRNAs, 5'ETS microRNAs are found at levels that are orders of magnitude lower than that of miR-4521, suggesting that they are also rapidly exported, and most of them have been recovered in extracellular vesicles.

Both miR-1275 and miR-6724 have been detected at high levels in circulating microRNAs from cancer patients and healthy individuals (*58, 59*). In bladder cancer, circulating miR-6724 is the most significantly upregulated of the 2565 microRNAs assayed (*8*), and in hepatocellular carcinoma, circulating miR-6724 is the most significantly upregulated of the 2588 microRNAs assayed (*7*). MiR-1275 was found to

be the most consistently upregulated of all microRNAs in tissue, plasma and urine samples, with a ROC curve area of 0.95 for urine, which confirms its exceptionally high abundance and diagnostic potential (*9*). Exosomes from PCa prostate cancer cells containing miR-1275 have been shown to accelerate the proliferation of osteoblasts in culture (*6*), and upregulation of miR-1275 promoted the invasion ability of squamous cell carcinoma of head and neck, where elevated levels predict poorer patient outcome (*60*). Google Scholar lists 2,610 citations for "miR-1275 cancer", and 1,780 citations for "mirR-1275 lung cancer", with >1000 citations for exosomes and for five other common cancers, which suggests that the extraordinarily high output of this 50-nt primary transcript is generally exploited by malignant cells. These observations support growing evidence that RNAPII hypertranscription is a general cancer driver (*13, 61*).

Methods

Alignment and processing of sequencing datasets to the T2T-CHM13 (hs1) and chm13_mini reference sequences.

Mini-chm13:

We constructed reference sequence chm13_mini from T2T-CHM13 version 2 (hs1) with these "chromosomes":

GART-SON	chr21:31,912,598-31,959,322 (46725 bp)
Hist_Chr1	chr1:148,935,900-149,012,900 (77001 bp)
Hist_Chr6	chr6:25,878,304-26,154,469 (276166 bp)
rDNA	hs1 chr21:3,141,168-3,185,955 (44788 bp)

To cleanly separate euchromatin from both rDNAs on the acrocentric p arms and 5S rDNA on Chromosome 1q, for some analyses, we constructed reference sequence chm13_mini3 T2T-CHM13 version 2 (hs1) with these "chromosomes":

GART-SON	chr21:31912597-31959322
Hist_Chr1	chr1:148935899-149012900
Hist_Chr6	chr6:25878303-26154469
RNA5Sr	chr1:227744287-228026142
rDNA	chr21:3141167-3185955x16
Chr1q-remaining	chr1:124048268-148935898 +
	chr1:149012901-227744286 +
	chr1:228026143-248387328

We downloaded Illumina fastq sequencing files from the NCBI SRA database.

Single-end sequencing

1. Trimmed adapters using cutadapt 4.9 with parameters: -q 20 -m 20 -a AGATCGGAAGAGC when appropriate
2. Aligned to reference sequences using bowtie2 2.5.4 with parameters: --end-to-end --very-sensitive --no-unal -q --phred33
3. Extracted mapped reads into bed file using bedtools bamtobed
4. Merged bed files for replicates (sort -m -k1,1 -k2n,2n -k3n,3n)
5. Separated bed files into plus/minus strands when appropriate (norm_strand.csh)
6. Computed fraction-normalized count tracks from bed files using bedtools genomecov (norm_beds.csh, fraction_norm.csh)

Paired-end sequencing

1. Trimmed adapters using cutadapt 4.9 with parameters: -m 20 --nextseq-trim 20 -a AGATCGGAAGAGCACACGTCTGAACTCCAGTCA -A AGATCGGAAGAGCGTCGTGTAGGGAAAGAGTGT -Z
2. Aligned to reference sequences using bowtie2 2.5.4 with parameters: --very-sensitive-local --soft-clipped-unmapped-tlen --no-unal --no-mixed --no-discordant --dovetail --phred33 -I 10 -X 1000
3. Extracted mapped reads into bed file using bedtools bamtobed.
4. Merged bed files for replicates (sort -m -k1,1 -k2n,2n -k3n,3n)
5. Separated bed files into plus/minus strands based on the strand of READ1 when appropriate
6. Computed fraction-normalized count tracks from bed files using bedtools genomecov (norm_beds.csh, fraction_norm.csh)

Datasets keyed to Figures

The following datasets were used in this study:

Fig. 1A-B: GSM8141208-GSM8141291
Fig. 1C: https://doi.org/10.5281/zenodo.13138686 DX_HS_P2S5_B*.bed.gz
Fig. 1D: https://doi.org/10.5281/zenodo.13138686 DX_HS_P2S5_M*.bed.gz
Fig. 2A-E, Fig. S5 PRO-seq: SRX11346954-11346955
Fig. 2F: TT-seq: GSM6755736-6755745
Fig. 3A-B: GSM9050852-53, GSM8180606-7, GSM8839021-9022, GSM8180614-15, GSM8180610-11, GSM8180618-19, GSM8839019-9020, GSM9095398, GSM8267449
Fig. 3C-D: GSM6043500, GSM6043501, GSM6043506, GSM6043507
Fig. 4A-B: GSM9050852-53, GSM9050854-55, GSM9050856-57, GSM9050858-59
Fig. 4C: GSM4296314, GSM4296315, GSM4296316, GSM4296317, GSM4296318, GSM4296319, GSM4296320
Fig. 5A: GSM4296337, GSM4296339, GSM4296321
Fig. 5B-C Human: GSM2265095, GSM2265098, GSM2265100
Fig. 5B-C Chimp: GSM2265102, GSM2265104, GSM2265106
Fig. 5B-C Macaque: GSM2265108, GSM2265109, GSM2265111
Fig. 6: GSM8791938-8791987, GSM8141208-8141291
Fig. 7 WT: GSM9000286-9000288 (merged)
Fig. 7 Pol3-inh: GSM9000289-9000291 (merged)
Fig. 7 Mock-inh: GSM9000274-9000277 (merged)
Fig. 7 DCGR8-inh: GSM9000282-9000285 (merged)
Fig. 7 Dicer-inh: GSM9000278-9000281 (merged)
Fig. S1–1-2: GSM2552214-2552220 (merged)
Fig. S1–3: GSM9095398
Fig. S1–4: GSM8267447
Fig. S1–5: GSM8267449
Fig. S1–6: GSM8267450
Fig. S1–7, Fig. S4: https://doi.org/10.5281/zenodo.13138686 DX_HS_P2S5_BC1_0429.bed.gz

Fig. S1–8: https://doi.org/10.5281/zenodo.13138686 DX_HS_P2S5_MA1_0401.bed.gz
Fig. S1–9: GSM8584120-8584125 (merged)
Fig. S1–10: GSM8584126-8584132 (merged)
Fig. S1–11: GSM1623148
Fig. S1–12: GSM1623146
Fig. S2: GSM3677824, GSM3677740-3677741, GSM36762-3677763, GSM3677784-3677785
Fig. S3: GSM5623305-5623317
Fig. S5: GSM8791938-8791987

Supplementary Table 1
Mini-chm13

Supplementary Software
Custom scripts used in this study are available from GitHub: https://github.com/Henikoff/Scripts.

Acknowledgments
We thank members of our lab and Toshio Tsukiyama for helpful discussions. This research was supported by the Howard Hughes Medical Institute (S.H.).

Declaration of interests
The authors declare no competing interests.

Author contributions
S.H. and J.G.H. performed the analyses. S.H. wrote the original draft. S.H. and J.G.H. reviewed and edited the draft.

References

1. R. W. Carthew, E. J. Sontheimer, Origins and Mechanisms of miRNAs and siRNAs *Cell* **136**, 642-655 (2009).
2. R. Drula, L. F. Ott, I. Berindan-Neagoe, K. Pantel, G. A. Calin, MicroRNAs from Liquid Biopsy Derived Extracellular Vesicles: Recent Advances in Detection and Characterization Methods *Cancers* **12**, (2020).
3. C. G. H. Ronnau *et al.*, Upregulation of miR-3195, miR-3687 and miR-4417 is associated with castration-resistant prostate cancer *World J. Urol.* **39**, 3789-3797 (2021).
4. G. E. Benoist *et al.*, Prognostic Value of Novel Liquid Biomarkers in Patients with Metastatic Castration-Resistant Prostate Cancer Treated with Enzalutamide: A Prospective Observational Study *Clin. Chem.* **66**, 842-851 (2020).
5. I. O. Fawzy *et al.*, miR-1275: A single microRNA that targets the three IGF2-mRNA-binding proteins hindering tumor growth in hepatocellular carcinoma *FEBS Lett.* **589**, 2257-2265 (2015).
6. Z. Zou, R. Dai, N. Deng, W. Su, P. Liu, Exosomal miR-1275 Secreted by Prostate Cancer Cells Modulates Osteoblast Proliferation and Activity by Targeting the SIRT2/RUNX2 Cascade *Cell Transplant.* **30**, 9636897211052977 (2021).
7. Y. Yamamoto *et al.*, Highly Sensitive Circulating MicroRNA Panel for Accurate Detection of Hepatocellular Carcinoma in Patients With Liver Disease *Hepatology communications* **4**, 284-297 (2020).
8. W. Usuba *et al.*, Circulating miRNA panels for specific and early detection in bladder cancer *Cancer Sci* **110**, 408-419 (2019).
9. M. A. Bustos *et al.*, Diagnostic miRNA Signatures in Paired Tumor, Plasma, and Urine Specimens From Renal Cell Carcinoma Patients *Clin. Chem.* **70**, 261-272 (2024).
10. N. Matyasovska *et al.*, Deep sequencing reveals distinct microRNA-mRNA signatures that differentiate pancreatic neuroendocrine tumor from non-diseased pancreas tissue *BMC cancer* **25**, 669 (2025).
11. E. L. Lim *et al.*, Comprehensive miRNA sequence analysis reveals survival differences in diffuse large B-cell lymphoma patients *Genome Biol* **16**, 18 (2015).
12. S. Henikoff *et al.*, Epigenomic analysis of Formalin-fixed paraffin-embedded samples by CUT&Tag *Nat Commun* **14**, 5930 (2023).
13. S. Henikoff *et al.*, RNA polymerase II at histone genes predicts outcome in human cancer *Science* **387**, 737-743 (2025).
14. G. Perez *et al.*, The UCSC Genome Browser database: 2025 update *Nucleic Acids Res* **53**, D1243-D1249 (2025).
15. S. J. Hoyt *et al.*, From telomere to telomere: The transcriptional and epigenetic state of human repeat elements *Science* **376**, eabk3112 (2022).
16. N. Altemose *et al.*, Complete genomic and epigenetic maps of human centromeres *Science* **376**, eabl4178 (2022).
17. A. Kozomara, M. Birgaoanu, S. Griffiths-Jones, miRBase: from microRNA sequences to function *Nucleic Acids Res* **47**, D155-D162 (2019).
18. M. Yoshikawa, Y. R. Fujii, Human Ribosomal RNA-Derived Resident MicroRNAs as the Transmitter of Information upon the Cytoplasmic Cancer Stress *BioMed research international* **2016**, 7562085 (2016).
19. D. B. Mahat *et al.*, Base-pair-resolution genome-wide mapping of active RNA polymerases using precision nuclear run-on (PRO-seq) *Nat Protoc* **11**, 1455-1476 (2016).
20. C. Antony *et al.*, Control of ribosomal RNA synthesis by hematopoietic transcription factors *Mol. Cell* **82**, 3826-3839 e3829 (2022).
21. B. Schwalb *et al.*, TT-seq maps the human transient transcriptome *Science* **352**, 1225-1228 (2016).
22. D. G. Altman, J. M. Bland, Measurement in medicine: the analysis of method comparison studies *The Statistician* **32**, 307-317 (1983).
23. J. E. Moore *et al.*, Expanded encyclopaedias of DNA elements in the human and mouse genomes *Nature* **583**, 699-710 (2020).
24. A. Lefebvre, T. Lecroq, H. Dauchel, J. Alexandre, FORRepeats: detects repeats on entire chromosomes and between genomes *Bioinformatics* **19**, 319-326 (2003).
25. Z. Wang *et al.*, The phosphatase PP1 sustains global transcription by promoting RNA polymerase II pause release *Mol. Cell* **84**, 4824-4842 e4827 (2024).
26. Q. Liu *et al.*, Identification of active miRNA promoters from nuclear run-on RNA sequencing *Nucleic Acids Res* **45**, e121 (2017).
27. T. Moss, J. C. Mars, M. G. Tremblay, M. Sabourin-Felix, The chromatin landscape of the ribosomal RNA genes in mouse and human *Chromosome Res.* **27**, 31-40 (2019).
28. S. Feng, J. L. Manley, Beyond rRNA: nucleolar transcription generates a complex network of RNAs with multiple roles in maintaining cellular homeostasis *Genes Dev.* **36**, 876-886 (2022).
29. M. S. Werner, A. J. Ruthenburg, Nuclear Fractionation Reveals Thousands of Chromatin-Tethered Noncoding RNAs Adjacent to Active Genes *Cell Rep* **12**, 1089-1098 (2015).
30. C. Herdman *et al.*, A unique enhancer boundary complex on the mouse ribosomal RNA genes persists after loss of Rrn3 or UBF and the inactivation of RNA polymerase I transcription *PLoS Genet* **13**, e1006899 (2017).
31. G. E. Zentner, A. Saiakhova, P. Manaenkov, M. D. Adams, P. C. Scacheri, Integrative genomic analysis of human ribosomal DNA *Nucleic Acids Res* **39**, 4949-4960 (2011).
32. B. M. Spector, J. F. Santana, M. A. Pufall, D. H. Price, DFF-ChIP: a method to detect and quantify

complex interactions between RNA polymerase II, transcription factors, and chromatin *Nucleic Acids Res* **52**, e88 (2024).
33. M. P. Meers, D. H. Janssens, S. Henikoff, Pioneer Factor-Nucleosome Binding Events during Differentiation Are Motif Encoded *Mol. Cell* **75**, 562-575 (2019).
34. J. F. Santana, G. S. Collins, M. Parida, D. S. Luse, D. H. Price, Differential dependencies of human RNA polymerase II promoters on TBP, TAF1, TFIIB and XPB *Nucleic Acids Res* **50**, 9127-9148 (2022).
35. J. C. Mars, M. Sabourin-Felix, M. G. Tremblay, T. Moss, A Deconvolution Protocol for ChIP-Seq Reveals Analogous Enhancer Structures on the Mouse and Human Ribosomal RNA Genes *G3* **8**, 303-314 (2018).
36. C. Grandori *et al.*, c-Myc binds to human ribosomal DNA and stimulates transcription of rRNA genes by RNA polymerase I *Nat Cell Biol* **7**, 311-318 (2005).
37. A. Arabi *et al.*, c-Myc associates with ribosomal DNA and activates RNA polymerase I transcription *Nat Cell Biol* **7**, 303-310 (2005).
38. S. S. Grewal, L. Li, A. Orian, R. N. Eisenman, B. A. Edgar, Myc-dependent regulation of ribosomal RNA synthesis during Drosophila development *Nat Cell Biol* **7**, 295-302 (2005).
39. J. M. Luppino *et al.*, Co-depletion of NIPBL and WAPL balance cohesin activity to correct gene misexpression *PLoS Genet* **18**, e1010528 (2022).
40. S. S. Rao *et al.*, A 3D map of the human genome at kilobase resolution reveals principles of chromatin looping *Cell* **159**, 1665-1680 (2014).
41. K. Jabbari, M. Chakraborty, T. Wiehe, DNA sequence-dependent chromatin architecture and nuclear hubs formation *Sci Rep* **9**, 14646 (2019).
42. S. Cruz-Ruiz, R. Vidal, M. Furlan-Magaril, J. T. Lis, M. Zurita, Transcriptional stress induces the overexpression of novel lncRNAs that regulate the BRCA1 locus *biorxiv* **doi: 10.1101/2025.03.11.642677**, (2025).
43. C. Dienemann, B. Schwalb, S. Schilbach, P. Cramer, Promoter Distortion and Opening in the RNA Polymerase II Cleft *Mol. Cell* **73**, 97-106 e104 (2019).
44. J. D. Parvin, B. M. Shykind, R. E. Meyers, J. Kim, P. A. Sharp, Multiple sets of basal factors initiate transcription by RNA polymerase II *J. Biol. Chem.* **269**, 18414-18421 (1994).
45. Y. Aoi *et al.*, NELF Regulates a Promoter-Proximal Step Distinct from RNA Pol II Pause-Release *Mol. Cell* **78**, 261-274 e265 (2020).
46. C. G. Danko *et al.*, Dynamic evolution of regulatory element ensembles in primate CD4(+) T cells *Nature ecology & evolution* **2**, 537-548 (2018).
47. H. R. Johnson *et al.*, The evolution of de novo human-specific microRNA genes on chromosome 21 *American journal of Biological Anthropology* **178**, 223–243 (2022).
48. A. R. Gruber, S. H. Bernhart, R. Lorenz, The ViennaRNA web services *Methods Mol. Biol.* **1269**, 307-326 (2015).
49. X. Liu *et al.*, Exosomes transmit T790M mutation-induced resistance in EGFR-mutant NSCLC by activating PI3K/AKT signalling pathway *Journal of cellular and molecular medicine* **24**, 1529-1540 (2020).
50. A. B. C. Geisen *et al.*, rDNA Copy Number Variation and Methylation During Normal and Premature Aging *Aging cell* **24**, e14497 (2025).
51. T. A. Potapova *et al.*, Chromosome-specific epigenetic control and transmission of ribosomal DNA arrays in Hominidae genomes *Cell genomics*, 101031 (2025).
52. Y. Hori, C. Engel, T. Kobayashi, Regulation of ribosomal RNA gene copy number, transcription and nucleolus organization in eukaryotes *Nat Rev Mol Cell Biol* **24**, 414-429 (2023).
53. K. Mizuno *et al.*, Intraindividual epigenetic heterogeneity underlying phenotypic subtypes of advanced prostate cancer *Nat Commun* **16**, 5543 (2025).
54. V. M. King, G. M. Borchert, MicroRNA Expression: Protein Participants in MicroRNA Regulation *Methods Mol. Biol.* **1617**, 27-37 (2017).
55. R. M. Sakhawala *et al.*, A noncanonical Pol III-dependent, Microprocessor-independent biogenesis pathway generates a germline-enriched miRNA family *Genes Dev.*, (2025).
56. J. W. Nicol, G. A. Helt, S. G. Blanchard, Jr., A. Raja, A. E. Loraine, The Integrated Genome Browser: free software for distribution and exploration of genome-scale datasets *Bioinformatics* **25**, 2730-2731 (2009).
57. R. D. Morin *et al.*, Application of massively parallel sequencing to microRNA profiling and discovery in human embryonic stem cells *Genome Res.* **18**, 610-621 (2008).
58. R. Manukonda *et al.*, Identifying Treatment Resistance Related Pathways by Analyzing Serum Extracellular Vesicles of Patients With Resistant Versus Regressed Retinoblastoma *Invest. Ophthalmol. Vis. Sci.* **64**, 26 (2023).
59. F. Zhou *et al.*, Circular RNA Protein Tyrosine Kinase 2 Promotes Cell Proliferation, Migration and Suppresses Apoptosis via Activating MicroRNA-638 Mediated MEK/ERK, WNT/beta-Catenin Signaling Pathways in Multiple Myeloma *Frontiers in oncology* **11**, 648189 (2021).
60. M. D. Liu *et al.*, MiR-1275 promotes cell migration, invasion and proliferation in squamous cell carcinoma of head and neck via up-regulating IGF-1R and CCR7 *Gene* **646**, 1-7 (2018).
61. M. Zatzman *et al.*, Widespread hypertranscription in aggressive human cancers *Sci Adv* **8**, eabn0238 (2022).

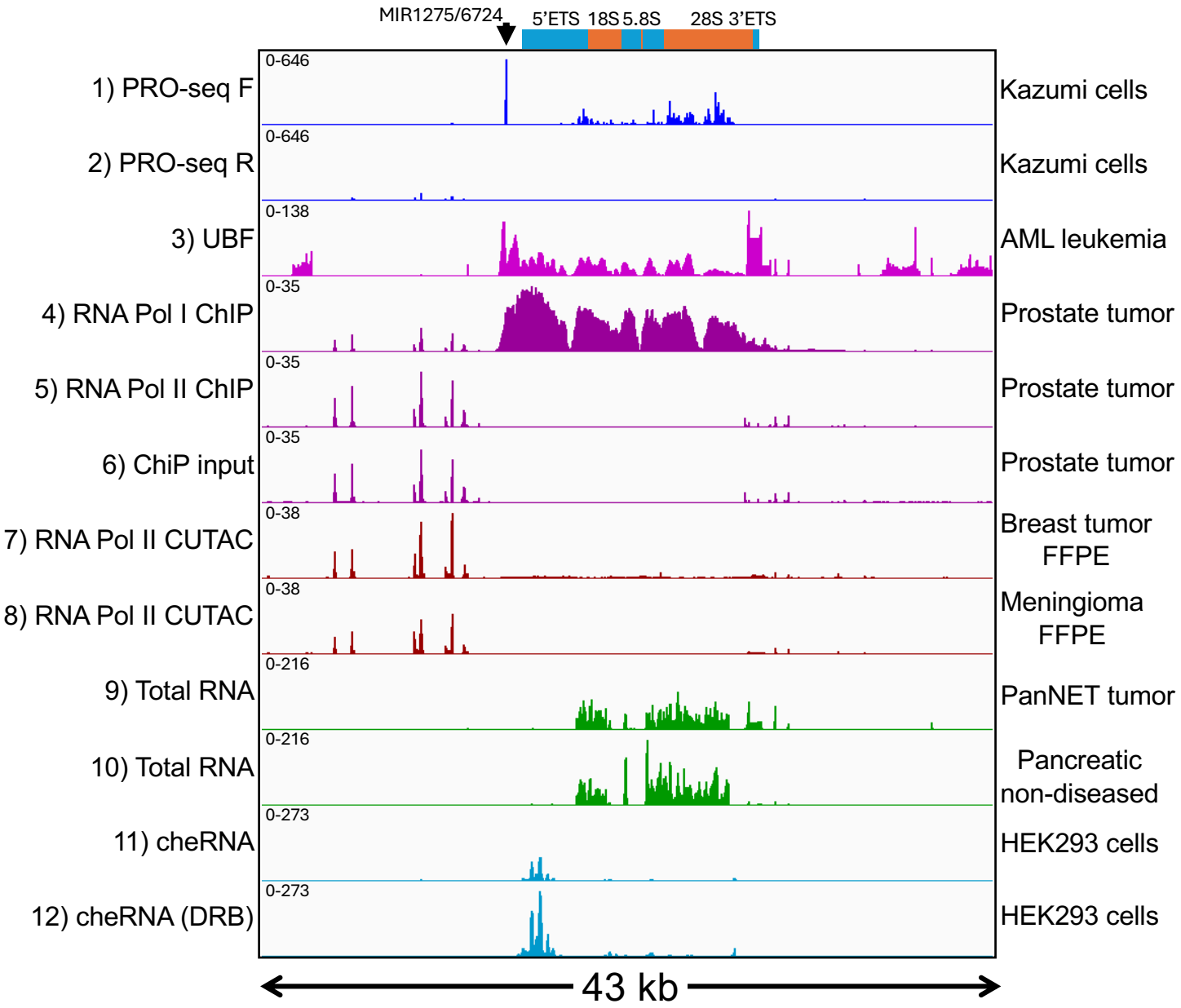

Fig. S1: Multi-modal profile alignments over the human rDNA repeat unit. PRO-seq forward stand signal is high over the transcribed region with a peak of maximum height just upstream. (**1-2**) PRO-seq data from Ref. (*26*) within a representative rDNA repeat unit (chr21:3,544,445-3,585,713); (**3**) UBF ChIP-seq data from GSM9095398; (**4-6**) RNAPI and RNAPII ChIP-seq data from GSM8267449; (**7-8**) RNA Pol II FFPE-CUTAC data from Ref. (*13*); (**9-10**) Total RNA data from Ref. (*10*); (**11-12**) chromatin-enriched RNA data from Ref. (*29*).

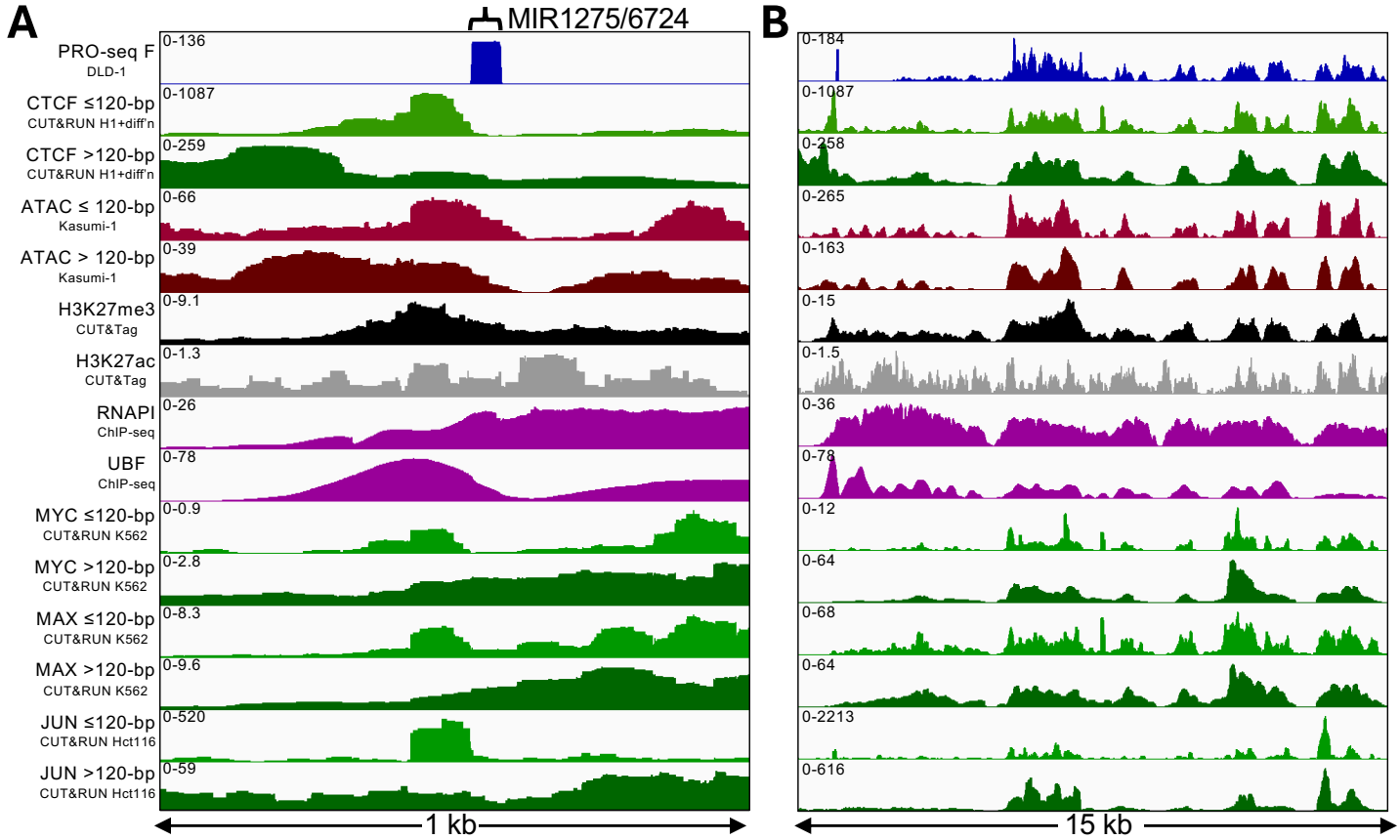

Fig. S2: Myc/Max and AP-1 Transcription Factors bind to the miR-1275/6724 promoter. Subnucleosomal CTCF fragments (≤120 bp, green) map immediately adjacent to the PRO-seq peak (blue) directly over the miR-1275/6724 DNA sequence and the major UBF peak, whereas nucleosomal CTCF peaks (>120 bp, dark green) map farther upstream, with little overlap. Merged reads are from human H1 embryonic cells and 3-4 days of differentiation. A similar pattern is seen for ATAC-seq reads (light and dark brown). In metastatic prostate cancer, the mark of Polycomb silencing, H3K27me3 (black), but not H3K27ac (grey) a mark of active chromatin, peaks over the miR-1275/6724-adjacent CTCF and UBF sites, which suggests that the shift of CTCF from direct binding to nucleosome binding upstream is accompanied by gain of an H3K27me3 nucleosome that silences the rDNA spacer promoters. K562 cell MYC, MAX and Hct116 JUN CUT&RUN fragments (light and dark brown) were profiled as controls and show co-occupancy with UBF and shift downstream. (**B**) Same as (A) expanded around the promoter and 5'ETS regions.

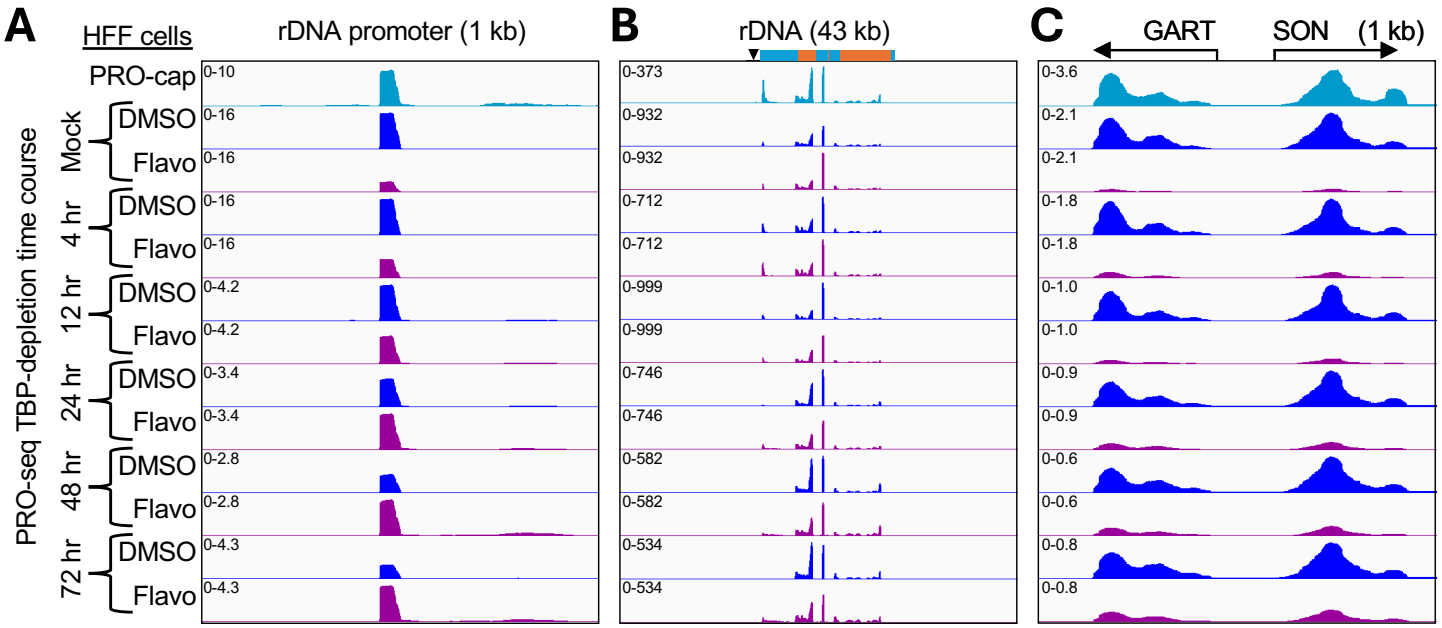

Fig. S3: Forward-strand PRO-cap and PRO-seq mini-chromosome profiles at the rDNA promoter (**A**), the full rDNA repeat (**B**), and the GART-SON control region (**C**), for DMSO- or Flavopiridol-treated cultures after PROTAC induction for the indicated times (*45*). When TBP-depletion time points are autoscaled, dramatic PRO-seq signal increases after Flavopiridol treatment are seen for the miR-1275/6724, compared to modest decreases for the GART/SON bidirectional promoters and modest increases for rDNA transcription.

MIR10401
Human -29.36
CGUGUGGGAAGGCGUGGGGUgcggaccccggcccg**ACCUCGCCGUCCCGCCCGCCG**
((.((((((.(((((.((((.(((...)))))))).))...))).)))))).))...
Chimp -31.78 kcal/mol
CGUGUGGGGGAGGCGUGUGGGGUGCGGAGCCCGGCCCG**ACCUCGCCGUCCCGCCCG**
.....(((((.((((.(((((((.(((.((...)))))))))))))))))).))).
Macaque -21.40 kcal/mol
GCGUUGGGAGGCACUGGGGUguggaacccggcccg**ACCUCGCUGUCCCGACCCCG**
..((((((((((...(((((.(((.....))))))))))).)))))))....

MIR663A
Human -50.00 kcal/mol
ccggcgucccc**AGGCGGGGCGCCGCGGGACCGC**ccucgugucuguggcggugggaucccgcggccguguuuuccugguggcccggccgugc
((((.((((((((.((.(((((((((((((((.(((.....))).)))))..)))))))).))).))..)))))).)))))))......
Chimp -51.39 kcal/mol
ccggcgucccgggc**GGGGCGCCGCGGGACCGCCCUC**gugucuguggcggugggaucccgcggccguguuuuccugguggcccggccgugc
((((.((((((((.((.(((((((((((((((.(((.....))).)))))..)))))))).))).))..)))))).)))))))......
Macaque -47.82 kcal/mol
ccggcgucccgggc**GGGGCGCCGCGGGACCGCCCUC**gugucuguggcggugggaucccgcggccguguuuuccugguggcccggccgugc
((((.((((((((.((.(((((((((((((((.(((.....))).)))))..)))))))).))).))..)))))).)))))))......

MIR3648
Human -54.85 kcal/mol
uggugggggg**AGCCGCGGGGAUCGCCGAGGG**ccggucggccgccccgggugccgcgcggugccgccggcggcggugaggccccgcgcgugug
..(((.((((.((((((.((..((((..((((.((....))))))..)))))).))))))((((((...))))))....)))).)))....
Chimp -54.07 kcal/mol
uggugggggg**AGCCGCGGGGAGCGCCGAGGG**ccggucggccgcuccgggugccgcgcggggccgccuucccgcucggaggcugccggcggu
....((((.((..(((((.((.((.((((((((....)))).)).)))))).)).)))))..)).)))).((((.(((.....))))))).
Macaque -46.50 kcal/mol
Ggcggtgggg**AGCCGCAGGGATCGCTGAAGG**cctggtcggccgctccaggtgccacgcggggccgccttcgtgctcggaggctgctggcgg
((((.(((((..((((..(((.((.....)))))...))))..)))))..)))).(((..(((.(((((((....))))))).))).))).

MIR3687 (no hairpin in miRBase)
Human: **CCCGGACAGGCGTTCGTGCGACGT**
**********+**
Chimp: **CCCGGACAGGCGTTCGTGCGATGT**
*****+****+**********
Macaque: **CCCGGGCAGGTGTTCGTGCGATGT**

MIR10396
Human -36.66 kcal/mol
GGCGGGGCUCGGAGCCGGGcuucggccg**GGCCCCGGGCCCUCGACCGGG**
((((((((((((.(((.(((....))).))).)))))))).)).))...
Chimp -41.45 kcal/mol
GGCGGGGCUCGGAGCCGGGcuucggccg**GGCUCCGGGCCCUCGACCGGA**
((((((((((((((((.(((....))).))))))))))))).)).))...
Macaque -35.33 kcal/mol
GCGGGGCUCGGAGCCGGGCcucggccg**GGCCCCGGGCCUCGACCGGA**
.((((((((((.(((.(((....))).))).))))))))))......

Fig. S4: MicroRNAs in the 5'ETS region are conserved in primates. RNAfold (*48*) was used to predict foldback structures for the five miRBase-annotated microRNAs in the 5'ETS region. Foldback structures are shown in Vienna format. expanded around the promoter and 5'ETS.

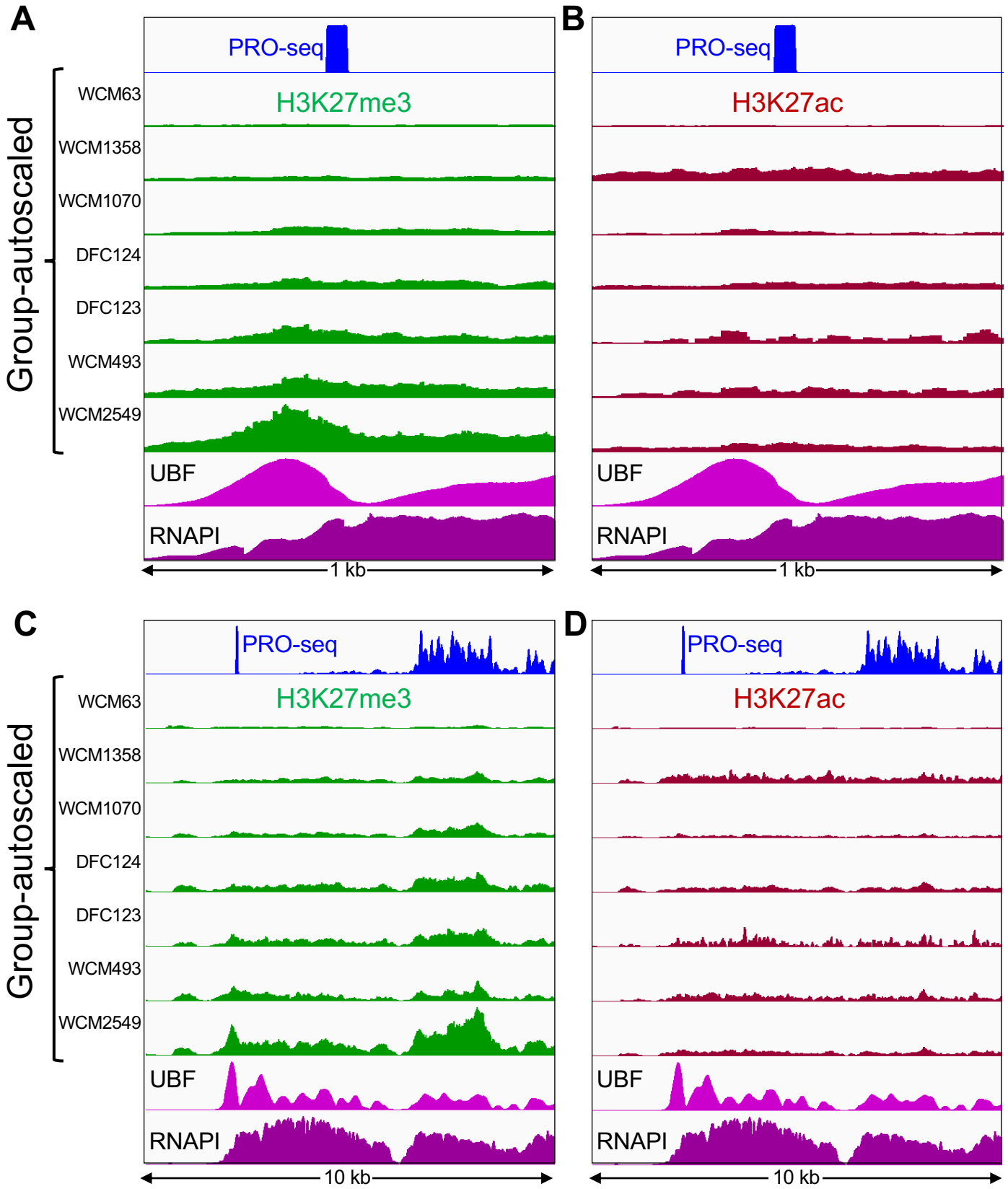

Fig. S5: H3K27me3-marked rDNA genes vary in abundance between prostate cancer metastases. High H3K27me3 (**A**) and low H3K27ac (**B**) over the RNAPI-transcribed regions from prostate metastases are consistent with densely packed RNAPIs on active copies and heterochromatic histone marks on silenced copies. CUT&Tag patient data from GSM8791938-GSM8791987 (*53*). Large variations in occupancy may reflect differences in both epigenetic and copy number differences between individuals (*50*). (**C-D**) Same as (A-B) expanded around the promoter and 5'ETS regions.